Photoactivity of shape-controlled TiO_2 in gas-solid regime under solar irradiation

Elisa I. García-López[a], Giuseppe Marcì[a], Maria Vittoria Dozzi[b], Leonardo Palmisano[a], Elena Selli[b,*]

[a] *Dipartimento di Energia, Ingegneria dell'Informazione e Modelli Matematici (DEIM), Viale delle Scienze, 90128 Palermo, Italy*

[b] *Dipartimento di Chimica, Università degli Studi di Milano, Via C. Golgi 19, 20133 Milano, Italy*

A B S T R A C T

Differently shape-controlled anatase TiO_2 materials were tested as photocatalysts under both simulated and natural solar irradiation. Their photocatalytic activity in 2-propanol and propene partial oxidation and in the complete mineralization of acetaldehyde appears to increase with decreasing the shape control of the TiO_2 material. This insight seems to be related to the residual presence of the templating species (fluoride anions) employed during the preparation of the shape-controlled TiO_2 materials. In fact, the calcination of the powders, leading to levelling of the fluoride ions content, but also to a remarkable surface area decrease, gave rise to an increase of photocatalytic activity per unit surface area of the materials. In these photocatalytic materials two opposing effects may concur in determining their photoactivity, i.e. the possibly beneficial effect of an increased extent of exposed {001} facets and the detrimental effect resulting from a larger amount of residual fluoride ions employed as capping agents.

Keywords: Photocatalysis; TiO_2; {001} facets; fluoride; capping agents.

---

* Corresponding author. *E-mail address:* elena.selli@unimi.it (E. Selli).

1. Introduction

The development of TiO_2 photocatalysts with high selectivity with respect to specific transformation and/or degradation of organics is very important for photocatalysis applications in both organic synthesis and environmental depollution fields. The opportunity to tune the selectivity of anatase crystals by modifying the surface properties of TiO_2, e.g. the percentage of exposed {001} facets, to produce morphologically controlled materials with peculiar, tailored photocatalytic properties has been extensively investigated in the last few years [1-3].

In particular, many efforts have been made in order to obtain materials with the less thermodynamically stable plate-like anatase TiO_2 morphology, i.e. characterized by a large content of {001} facets, which can be obtained mainly by adding proper capping agents during its crystal growth. However, the residual presence of such templating species on the TiO_2 surface may significantly affect the photocatalyst properties, thus preventing an accurate evaluation of the intrinsic effects of each specific type of 'clean' anatase crystal facet. This is for example the case of fluoride anions, which still represent the most effective and commonly used agents employed to stabilize {001} facet enriched anatase TiO_2 [4]. In fact, TiO_2 surface fluorination has been shown to remarkably affect not only the adsorption mode and extent of reactants on the TiO_2 surface, and consequently the production of active species, but also photoproduced charge separation and surface transfer, as well as the kinetics and mechanism of surface photocatalytic reactions [5-9]. In particular, extensive studies evidenced that the rate of photocatalytic oxidation reactions

may either increase or decrease upon TiO_2 fluorination, depending on the prevailing oxidation mechanism [10-18].

At the same time a remarkable synergistic effect was recently outlined in ammonia oxidation photoactivity, induced by combining the exposure of a relatively high percentage of TiO_2 {001} facets with their surface fluorination [19]. This prompted us to systematically compare the performance attained in other gas phase photocatalytic oxidation reactions by two series of shape-controlled TiO_2 materials [20], either before or after the removal of the fluoride capping agent. Such materials were previously prepared, fully characterized and tested by some of us in the exposed-facet-dependent photocatalytic oxidation of formic and terephthalic acids. The primary role played by fluoride removal through calcination in making {001} facets effectively photoactive was clearly outlined.

In the present work, the photocatalytic activity of such shape-controlled materials either before or after calcination to remove fluoride ions was investigated in three gas-solid oxidation reactions under solar irradiation. In particular, 2-propanol partial oxidation under simulated solar light was investigated as a typical test reaction in the gas-solid regime [21-22]. Propene partial oxidation was investigated mainly to check if and how different exposed TiO_2 facets may affect the selective epoxidation of propene [23]. Complete acetaldehyde mineralization under solar irradiation was studied because it is a simple reaction occurring from the frequently encountered acetaldehyde intermediate oxidation species, directly leading to its complete photocatalytic degradation into CO_2 and H_2O.

2. Experimental

2.1. Photocatalysts preparation

Starting from the previously optimized hydrothermal route [20], anatase crystals with different degrees of truncation were obtained by adding different volumes of a 48 wt.% HF aqueous solution and of water to 5.0 mL of titanium isopropoxide contained in a Teflon liner, up to a 5.6 mL final volume. After 15 min stirring, the resulting mixture was transferred into a stainless-steel autoclave, which was closed and heated at 180 °C in an electric oven for 24 h. Once cooled naturally to room temperature, the precipitate was washed several times with water until the fluoride ion concentration, determined by ion chromatography with conductivity detection (Metrohm 761 Compact IC), was below 5 ppm.

The so-obtained materials were labelled as HT_X, where HT refers to the employed hydrothermal preparation method, and X stands for the nominal F/Ti molar ratio, ranging from 0.1 to 1.0. A reference sample, named HT_0, was also prepared under the same conditions by simply adding 0.6 mL of water (and no HF) to titanium isopropoxide. Aiming at removing the surface fluoride employed as capping agent during the synthesis, a portion of all HT samples was calcined in air at 500 °C for 2 h; the so-obtained photocatalysts were labelled HT_X_500.

All reagents were purchased from Aldrich and employed as received. Water purified by a Milli-Q water system (Millipore) was used throughout.

2.2. Photocatalysts characterization

X-ray powder diffraction (XRPD) patterns were collected on a Panalytical X'Pert Pro diffractometer, using Ni- filtered Cu Kα radiation, at a scan rate of 0.05 deg s^{-1}. Crystal phase determination, line profile analysis based on Rietveld refinement and calculations for determining the relative percent of {001} facets of the investigated materials were performed as already described in detail [20,24].

Nitrogen adsorption−desorption data were collected at 77 K using a Micromeritics Tristar II 3020 V1.03 apparatus after outgassing at 300 °C for 1 h under a N_2 stream. Specific surface area (SSA) values were obtained by applying the Brunauer−Emmett−Teller (BET) method to the adsorption isotherms.

X-ray photoemission spectroscopy (XPS) data were collected in a multi-technique ultrahigh-vacuum (UHV) chamber (base pressure 1.0×10^{-9} mbar) equipped with a VG MKII ESCALAB electron analyzer (5 channeltrons). Measurements were made at room temperature in normal emission using a non-monochromatized Mg anode X-ray source (hν = 1253.6 eV). Powder samples were suspended in bi-distilled water and drop-cast on high-purity copper foils. After drying in air, the obtained films were introduced into the UHV chamber and outgassed overnight. The charging observed during measurements was corrected by aligning the Ti $2p_{3/2}$ core-level peak signal to 459.0 eV.

The diffuse reflectance spectra (DRS) were recorded in air at room temperature in the 250-800 nm wavelength range using a Shimadzu UV-2401 PC spectrophotometer, with $BaSO_4$ as the reference material.

2.3. Photocatalytic tests

The photoreactivity of the powders was studied in the gas-solid regime by using two photocatalytic set-ups under either simulated or natural solar irradiation. The degradation of 2-propanol was investigated in a saturated O_2 atmosphere employing a 25 mL cylindrical Pyrex batch photoreactor, under the simulated solar irradiation produced by a Solarbox apparatus (1500 W high pressure Xenon lamp). The photocatalyst powders (60 mg) were irradiated from the top. The employed set-up is reported elsewhere [25]. Liquid 2-propanol was injected into the photoreactor (nominal initial concentration 1.56×10^{-3} M) and irradiation was started only after steady state conditions were achieved. The runs lasted ca. 2.5 h.

The photocatalytic oxidation of both propene and acetaldehyde was investigated under natural outdoor solar light in a saturated O_2 atmosphere by using the same gas-solid regime photoreactor used for 2-propanol oxidation. The solar irradiance reaching the photoreactor was measured each minute by means of a radiometer. From these data, the cumulative photon energy reaching the reactor was calculated. By this way the photoactivity of the different photocatalysts could be evaluated under different natural sunlight irradiation conditions. The initial concentration of propene was 3.2×10^{-3} M and that of acetaldehyde was 1.0×10^{-3} M.

For all of the experiments, irradiation started only after the adsorption equilibrium of the substrate onto the photocatalyst surface was attained in the dark. The reaction was monitored by withdrawing gas samples from the photoreactor by means of a gas-tight syringe during the runs. The reacting fluid was analyzed in a Shimadzu 2010 gas

chromatograph (GC) equipped with a Phenomenex Zebron Wax-plus. CO_2 was analyzed by a HP 6890 Series GC equipped with a packed column GC 60/80 Carboxen-1000 and a TCD.

3. Results and discussion

3.1. Photocatalyst characterization

XRPD analysis confirmed the full anatase phase composition of the investigated TiO_2 photocatalysts, belonging to both HT and HT_500 series (see Figure 1). The progressive increase of fluorine amount employed during the synthesis determined a clear morphological evolution towards the stabilization of {001} facets-enriched anatase nanoparticles, also confirmed by HR-TEM analysis, as shown in Figure 2. In particular, the percent amount of exposed {001} facets of HT_X samples increased with increasing the fluorine content up to F/Ti = 1.0, while calcination at 500 °C caused a general decrease of the amount of such facets (Table 1), with the consequent conversion of the original plate-like shape of nanocrystals to a slightly more isotropic one. In particular, the crystal shape of HT_1 was essentially preserved even after thermal treatment, though nanocrystals appeared more irregular, as evidenced in the HR-TEM images (see Figure 2 and other images reported in ref. 20).

The uncalcined HT photocatalyst series exhibited similar SSA, slightly increasing with increasing fluorine content, from 80 $m^2\ g^{-1}$ for F/Ti = 0 to 92 $m^2\ g^{-1}$ for F/Ti = 1.0. Calcination of course produced an expected decrease in SSA due to crystallite sintering. Some SSA variation can be appreciated within the HT_500 photocatalyst series, all SSA values of the samples with $0 \leq F/Ti \leq 1$ being in the 50–59 $m^2\ g^{-1}$ range (Table 1).

XPS analysis confirmed a progressive increase of surface fluoride amount with increasing F/Ti ratio in the HT series, all samples being characterized by a F 1s XPS signal centred at about 684.5 eV, arising from terminal Ti−F bonds. A significantly lower, quite uniform F-coverage was detected in the HT_500 series [20], which confirms that annealing at 500 °C is an efficient route to almost totally remove the residual fluoride capping agent (Table 1). No XPS signal due to lattice fluorine could be detected in the samples, though its presence cannot be excluded. Indeed, low amounts of fluorine in the lattice of similar materials have been recently shown to induce the formation of EPR detectable reduced Ti(III) centres that localize the extra electron needed for charge compensation [26].

The diffuse reflectance spectra of the investigated photocatalysts (see Figures 3A and B) show the usual absorption onset of anatase at $\lambda < 400$ nm. The different crystal size could be responsible for the observed absorption discrepancies, even more than the percentage of exposed {001} facets. The heat treatment at 500 °C eliminates the absorption contribution extending over the whole visible range, possibly originated from residual surface carbon after the synthesis and mainly evidenced in the case of HT_0.1 and HT_0.5.

The optical band gap energy E_{gap} of the materials was evaluated from the diffuse reflectance spectra employing the Kubelka-Munk function $F(R\infty)$, by extrapolating a linear fitting in the Tauc plot [27], i.e the $(F(R'\infty)\cdot E)^{1/2}$ plot vs. incident light energy (in eV) and considering TiO_2 as an indirect semiconductor. The obtained E_{gap} values were ca. 3.2 eV for all samples.

3.2. Photocatalytic activity

3.2.1 2-Propanol photocatalytic degradation under simulated solar irradiation

The photocatalytic runs started after the system achieved the steady state conditions under dark conditions. The initial substrate concentration measured after equilibration was always much lower than the nominal one, indicating that 2-propanol was partially adsorbed on the photocatalyst surface. Preliminary tests showed that 2-propanol degradation occurred only under irradiation and in the presence of both photocatalyst and oxygen. Figures 4 and 5 report the concentration of 2-propanol and of its partial oxidation products vs. the irradiation time in runs carried out in the presence of uncalcined and calcined photocatalysts, respectively. The data reported in Figures 4 and 5 are the average values obtained in three different runs.

All samples were able to photo-oxidize 2-propanol under the investigated irradiation conditions, producing propanone and acetaldehyde as intermediate species along with CO_2 as the final oxidation product. In fact, 2-propanol concentration decreased under irradiation and a simultaneous increase of propanone concentration was observed along with the production of low amounts (traces in some cases) of acetaldehyde.

A perusal of Figures 4 and 5 highlights that the apparent rate of 2-propanol disappearance was lower than the apparent rate of propanone formation. This can be explained by considering that under irradiation, 2-propanol underwent both photocatalytic oxidation and simultaneous photo-thermal desorption from the photocatalyst surface. Consequently, the photoactivity of the various photocatalysts in this reaction was compared by considering the initial rate (during the first 20 min) of propanone formation (r_{pro}).

The results are reported in Table 2. Both photocatalysts prepared in the absence of fluoride anion (either uncalcined or calcined, i.e. HT_0 and HT_0_500) were found to be most active and, interestingly, the thermal treatment of HT_0 led to a performance increase.

On the contrary, the photoactivity of fluorine-containing samples did not vary, or it slightly decreased apparently, after the calcination step required to remove surface fluoride.

However, it is worth recalling that upon calcination the SSA of the materials largely decreased (see Table 1) and that the rate of propanone formation per unit area should better be considered to evaluate the effects of surface fluorination on the photoactivity of the here investigated differently faceted anatase TiO_2 materials. Table 2 reports the rate of propanone formation per unit area (r_{pf}) determined with the here investigated photocatalysts series. A beneficial effect of calcination is clearly outlined for HT_0, possibly due to increased crystallinity of the material, and for the HT_X series with X > 0.1, pointing to an increased adsorption of the organic substrate on the photocatalyst surface after fluoride partial removal, which is beneficial in terms of photoactivity per unit surface area of the materials.

Figures 4 and 5 also show that the mass balance of carbon was not completely fulfilled during the course of the photocatalytic reaction, indicating that part of the substrate and eventually also of the oxidation intermediates remained adsorbed on the photocatalyst surface. The presence of small amounts of acetaldehyde indicate that a C-C bond oxidative breaking also occurred in 2-propanol. However, by considering the amount of CO_2 detected in the gas phase at the end of each run, the amount of carbon-containing species remained adsorbed on the catalyst surface was always negligible.

3.2.2. Propene and acetaldehyde oxidation under natural solar irradiation

In the experiments performed under natural solar light, the irradiation intensity may of course change during the experiment, as well as also from day to day. Consequently, a

comparison between the results obtained in different runs is possible only if the overall photon energy impinging on the reactor during each photocatalytic run is taken into account. This latter was calculated as already detailed [28,29], by measuring the irradiance during each experimental run.

The photoactivity experiments started after steady state conditions were achieved in the dark, i.e. when the concentration of propene remained constant with time (ca. 0.5 h). No adsorption phenomena were evidenced for the propene molecule in the dark, probably due to its apolar nature. Acetaldehyde, propylene oxide, propanone, acrolein and methanol were found to form during propene photocatalytic partial oxidation, along with CO_2 as the final oxidation product, as in previous studies that some of us carried out using TiO_2/SiO_2 [30] and $SrTiO_3$ based perovskites [31]. Figure 6 reports the propene conversion profiles vs. the cumulative photon energy on the reactor in runs carried out in the presence of the here investigated TiO_2–based photocatalysts.

With non-calcined photocatalysts (Figure 6A) the highest propene oxidation rate was observed in the presence of HT_0, with ca. 92% propene conversion after ca. 210 J light energy impinging the reactor (3 h-long solar irradiation), whereas a ca. 70 % propene conversion was attained in the presence of HT_0.1, HT_0.5 and HT_1 at the same cumulative energy value. Calcination of the materials gave rise to a levelling effect as far as propene conversion is concerned (Figure 6B), with the only exception of the HT_1_500 photocatalyst, for which propene conversion was much lower than that observed with non-calcined HT_1 and also with the other calcined materials. Indeed, a certain deactivation in propene conversion seems to occur at ca. 180 J (2 h-long irradiation). During these runs, small amounts of partial propene oxidation products (i.e. acetaldehyde, propene oxide,

propanone, acrolein and methanol) were formed. Notably, we observed that, among the uncalcined photocatalysts, HT_0 gave rise to the maximum selectivity towards propene oxide formation. On the contrary, by increasing the amount of fluoride in uncalcined photocatalyst samples, a gradual increase in selectivity towards the formation of acetaldehyde and methanol was observed. In general, the annealing treatment of the fluorine-containing materials seems to have no effect on both their photoactivity and selectivity.

Due to the small differences in photoactivity observed among the various photocatalysts, only selected photocatalysts, i.e. HT_0 and HT_1, containing either no fluoride or the maximum amount of fluoride, and the corresponding calcined HT_0_500 and HT_1_500 samples, having an almost identical SSA, were tested in photocatalytic experiments of acetaldehyde oxidation. Adsorption of the substrate under dark conditions was observed in the case of both photocatalysts. No acetaldehyde degradation intermediate species were observed, apart from traces of methanol. Due to the strong adsorption of this substrate on the two photocatalysts, their activity could not be evaluated in terms of acetaldehyde disappearance, but it was evaluated in terms of CO_2 formation rate, which was 7.8×10^{-6} M J^{-1} with both HT_0 and HT_1. On the other hand, CO_2 production occurred at a slightly higher rate with the calcined HT_0_500 and HT_1_500 photocatalysts (8.4×10^{-6} and 8.1×10^{-6} M J^{-1}, respectively). Also in this case, by taking into account the reduced SSA of the calcined materials, the rate of CO_2 production per unit photocatalyst surface area can be calculated. The so obtained values indicate a ca. 70% activity per surface area increase upon surface fluoride removal by calcination, perfectly in line with the results reported in

Table 2 for propanone formation in 2-propanol photocatalytic oxidation. This confirms that surface fluoride has a detrimental effect on photoactivity also in the case of acetaldehyde photocatalytic oxidation.

4. Conclusions

Present results obtained in gas-solid regime reactions employing TiO_2 anatase photocatalysts with different percentage of exposed {001} facets do not lead to an uncontroversial correlation between photoactivity and morphology of the materials, which was found instead with the same series of differently faceted anatase photocatalysts in the photocatalytic oxidation of formic acid and terephthalic acids in aqueous suspension [20]. In that case an important role might have been played by the aqueous solvent, from which active species such as hydroxyl radicals may be produced on the photocatalyst surface under irradiation, allowing oxidation mechanisms different from the direct electron transfer paths occurring in gas-solid phase photocatalytic reactions. Present results indicate that the activity of differently shape controlled TiO_2 anatase photocatalysts need to be interpreted in the light of two possibly opposing effects, i.e. the different intrinsic reactivity of the exposed facets and the hindered organic substrate adsorption on the surface containing residual fluoride ions from the synthesis, which has detrimental effects on photoactivity.

Acknowledgments

This work received support from the Fondazione Cariplo Project *Novel Photocatalytic Materials Based on Heterojunctions for Solar Energy Conversion* (grant 2013-0615). The

use of instrumentation purchased through the Regione Lombardia-Fondazione Cariplo joint *SmartMatLab* project (Fondazione Cariplo grant 2013-1766) is also acknowledged.

References

[1] G. Liu, H.G. Yang, J. Pan, Y.Q. Yang, G.Q. Lu, H. Cheng, Chem. Rev. 114 (2014) 9559–9612.

[2] M.V. Dozzi, E. Selli, Catalysts 3 (2013) 455–485.

[3] M. Maisano, M.V. Dozzi, E. Selli, J. Photochem. Photobiol. C: Photochem. Rev. 28 (2016) 29–43.

[4] H.G. Yang, C.H. Sun, S.Z. Qiao, J. Zou, G. Liu, S.C. Smith, H.M. Cheng, G.Q. Lu, Nature 45 (2008) 638–641.

[5] H. Park, W. Choi, J. Phys. Chem. B 108 (2004) 4086–4093.

[6] M. Mrowetz, E. Selli, Phys. Chem. Chem. Phys. 7 (2005) 1100–1102.

[7] M. Mrowetz, E. Selli, New J. Chem. 30 (2006) 108–114.

[8] V. Maurino, A. Bedini, M. Minella, F. Rubertelli, E. Pelizzetti, C. Minero, J. Adv. Oxid. Technol. 11 (2008) 184–192.

[9] M.-V. Sofianou, V. Psycharis, N. Boukos, T. Vaimakis, J. Yu, R. Dillert, D. Bahnemann, C. Trapalis, Appl. Catal. B: Environ. 142 (2013) 761–768.

[10] M.S. Vohra, S. Kim, W. Choi, J. Photochem. Photobiol. A: Chem. 160 (2003) 55–60.

[11] Y.C. Oh, W.S. Jenks, J. Photochem. Photobiol. A: Chem. 162 (2004) 323–328.

[12] K. Lv, Y. Xu, J. Phys. Chem. B 110 (2006) 6204–6212.

[13] Y. Xu, K. Lv, Z. Xiong, W. Leng, W. Du, D. Liu, X. Xue, J. Phys. Chem. C 111 (2007) 19024–19032.

[14] J. Tang, H. Quan, J. Ye, Chem. Mater. 19 (2007) 116–122.

[15] D. Monllor-Satoca, R. Gomez, J. Phys. Chem. C 112 (2008) 139–147.

[16] Q. Wang, C. Chen, D. Zhao, W. Ma, J. Zhao, Langmuir 24 (2008) 7338–7345.

[17] J. Yu, W. Wang, B. Cheng, B.L. Su, J. Phys. Chem. C 113 (2009) 6743–6750.

[18] M.V. Dozzi, G.L. Chiarello, E. Selli, J. Adv. Oxid. Technol. 13 (2010) 305–312.

[19] M. Chen, J. Ma, B. Zhang, G. He, Y. Li, C. Zhang, H. He, Appl. Catal. B: Environ. 207 (2017) 397–403.

[20] M. Maisano, M.V. Dozzi, M. Coduri, L. Artiglia, G. Granozzi, E. Selli, ACS Appl. Mater. Interfaces 8 (2016) 9745–9754.

[21] [G. Marcì, E. García-López, G. Mele, L. Palmisano, G. Dyrda, R. Słota, Catal. Today 143 (2009) 203–210.

[22] M. Sbouia, S. Bouattoura, L.F. Liotta, V. La Parola, M. Gruttadauria, G. Marcì, S. Boufie, J. Photochem. Photobiol. A: Chem. 350 (2018) 142–151.

[23] E. García-López, G. Marcì, B. Megna, F. Parisi, L. Armelao, A. Trovarelli, M. Boaro, L. Palmisano, J. Catal. 321 (2015) 13–22.

[24] M. Coduri, M. Maisano, M.V. Dozzi, E. Selli, Z. Phys. Chem. 230 (2016) 1233–1248.

[25] G. Marcì, E. García-López, L. Palmisano, Catal. Commun. 53 (2014) 38–41.

[26] Z. Barbieriková, D. Dvoranová, M.-V. Sofianou, C. Trapalis, V. Brezová, J. Catal. 331 (2015) 39-48.

[27] J. Tauc, Mater. Res. Bull. 5 (1970) 37–46.

[28] F. Méndez-Arriaga, M.I. Maldonado, J. Gimenez, S. Esplugas, S. Malato, Catal. Today 144 (2009) 112–116.

[29] M. Ilkaeva, I. Krivtsov, E.I. García-López, G. Marcì, O. Khainakova, J.R. García, L. Palmisano, E. Díaz, S. Ordóñez, J. Catal. 359 (2018) 212–222.

[30] M. Rico-Santacruz, E. Serrano, G. Marcì, E. I. García-López, J. García-Martínez, Chem. Eur. .J. 21 (2015) 18338–18344.

[31] E.I. García-López, G. Marcì, B. Megna, F. Parisi, L. Armelao, A. Trovarelli, M. Boaro, L. Palmisano, J. Catal. 321 (2015) 13–22.

Table 1

Percent amount of exposed {001} facets, specific surface area (SSA) and atomic percent content of surface fluorine (F_{surf}) of the HT_X and HT_X_500 photocatalyst series.[a]

Sample	{001} (%)	SSA ($m^2\ g^{-1}$)	F_{surf} (%)
HT_0	7.3 ± 0.6	80.0 ± 0.6	-
HT_0.1	13.7 ± 0.7	81.4 ± 0.9	4.0
HT_0.5	53.4 ± 0.6	84.3 ± 1.0	3.6
HT_1	82.3 ± 0.8	92.3 ± 0.9	6.5
HT_0_500	9.8 ± 0.5	54.9 ± 0.7	-
HT_0.1_500	14.3 ± 0.5	59.0 ± 0.8	1.6
HT_0.5_500	40.2 ± 0.6	49.3 ± 0.2	3.0
HT_1_500	59.3 ± 0.8	55.5 ± 0.5	1.8

[a] All values are taken from Ref. 20.

Table 2

Initial rate of propanone formation (r_{pro}) from 2-propanol photocatalytic oxidation and rate of propanone formation per unit photocatalyst surface area (r_{pf}), obtained in the presence of the here investigated photocatalyst series.

Uncalcined samples	$r_{pro} \times 10^5$ ($M\ min^{-1}$)	$r_{pf} \times 10^7$ ($M\ min^{-1}\ g\ m^{-2}$)	Calcined samples	$r_{pro} \times 10^5$ ($M\ min^{-1}$)	$r_{pf} \times 10^7$ ($M\ min^{-1}\ g\ m^{-2}$)
HT_0	4.0	5.0	HT_0_500	4.8	8.7
HT_0.1	3.2	4.0	HT_0.1_500	2.2	3.7
HT_0.5	2.1	2.5	HT_0.5_500	1.9	3.8
HT_1	2.0	2.1	HT_1_500	1.9	3.6

Figure captions

Figure 1. XRPD patterns of (A) the HT and (B) the HT_500 photocatalyst series.

Figure 2. HR-TEM images of (A) HT_0, (B) HT_1 and (C) HT_1_500.

Figure 3. (A) Diffuse reflectance spectra (DRS) of (a) HT_0, (b) HT_0.1, (c) HT_0.5 and (d) HT_1; (B) DRS of (a) HT_0_500, (b) HT_0.1_500, (c) HT_0.5_500 and (d) HT_1_500.

Figure 4. Time-course of (♦) 2-propanol, (■) propanone and (▲) acetaldehyde concentration vs. time under simulated solar radiation in 2-propanol photocatalytic oxidation in the presence of the uncalcined photocatalysts.

Figure 5. Time-course of (♦) 2-propanol, (■) propanone and (▲) acetaldehyde concentration vs. time under simulated solar radiation in the presence of the calcined photocatalysts.

Figure 6. Time-course of propene conversion vs. the cumulative photon energy (naural solar radiation) in the presence of (A) non calcined photocatalysts (♦) HT_0; (■) HT_0.1; (▲) HT_0.5; (●) HT_1, and (B) calcined photocatalysts (♦) HT_0_500; (■) HT_0.1_500; (▲) HT_0.5_500; (●) HT_1_500.

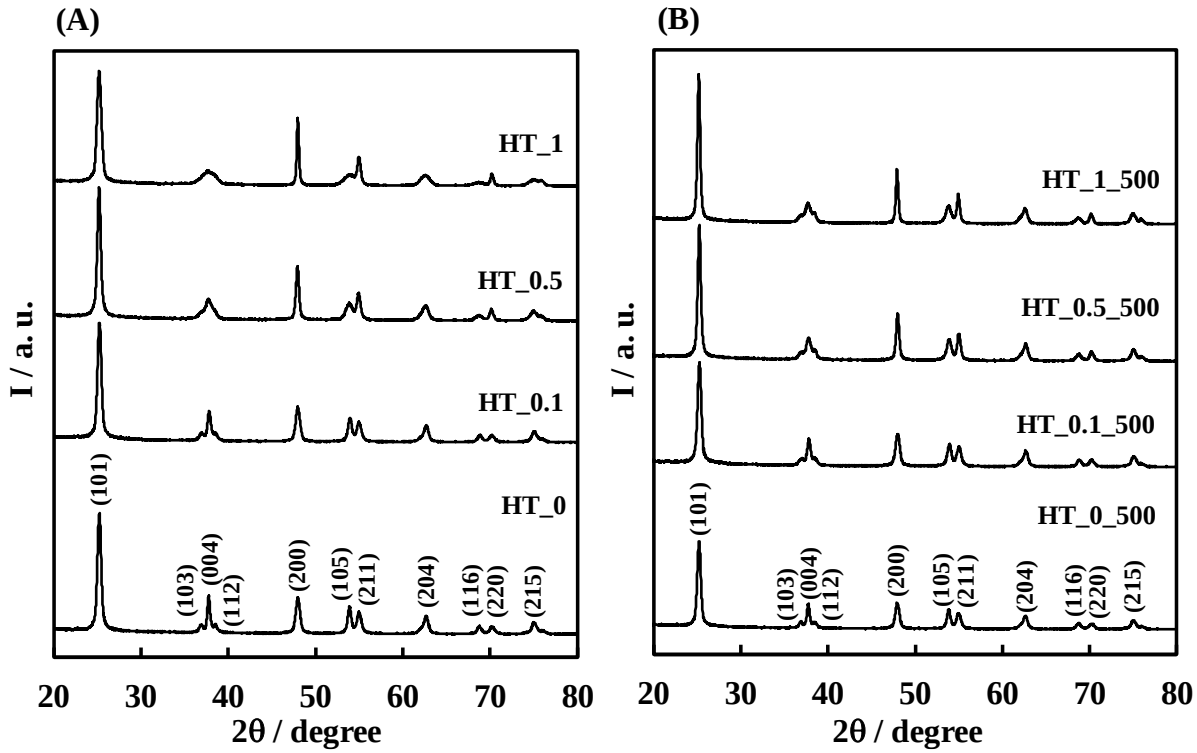

Figure 1. XRPD patterns of (A) the HT and (B) the HT_500 photocatalyst series.

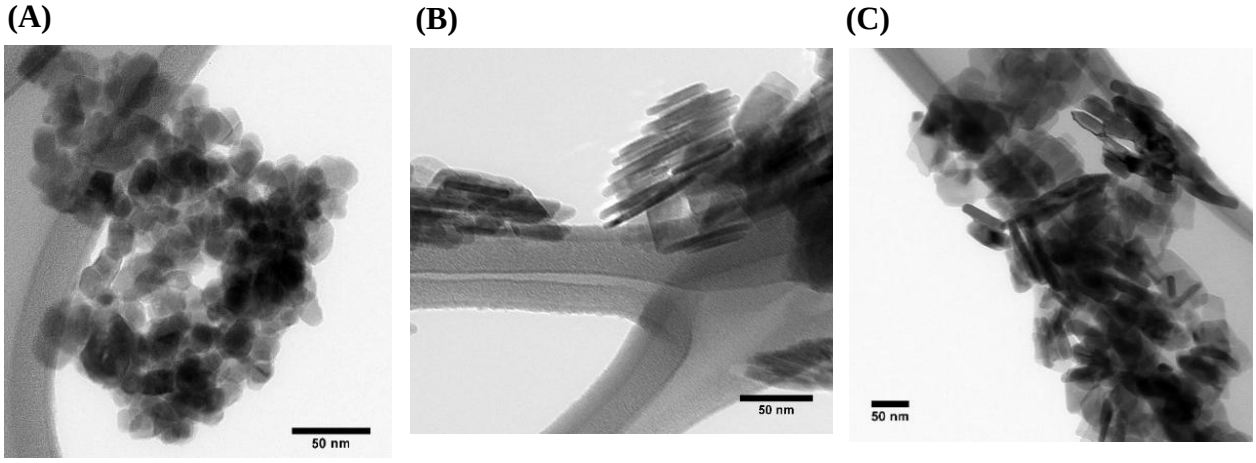

Figure 2. HR-TEM images of (A) HT_0, (B) HT_1 and (C) HT_1_500.

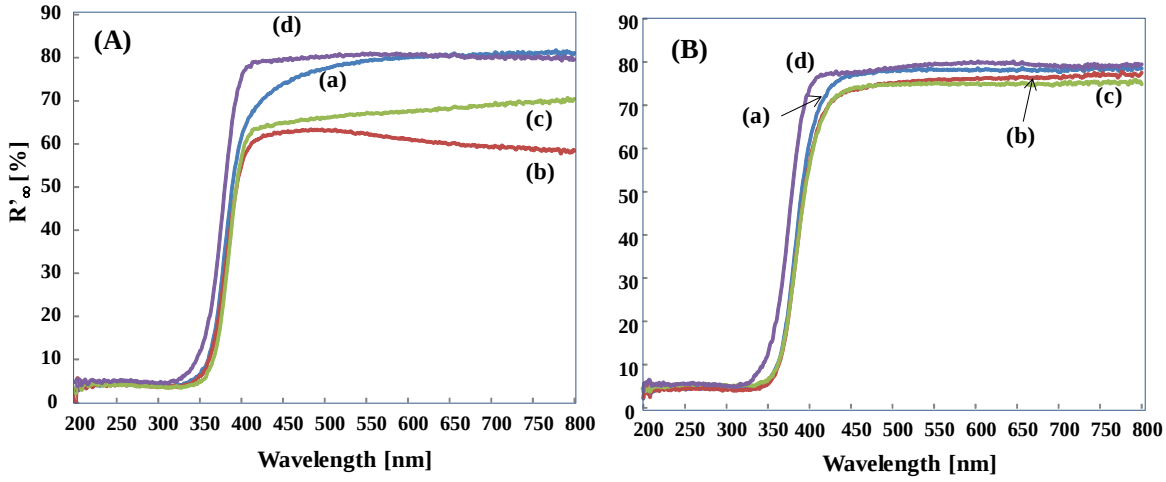

Figure 3. (A) Diffuse reflectance spectra (DRS) of (a) HT_0, (b) HT_0.1, (c) HT_0.5 and (d) HT_1; (B) DRS of (a) HT_0_500, (b) HT_0.1_500, (c) HT_0.5_500 and (d) HT_1_500.

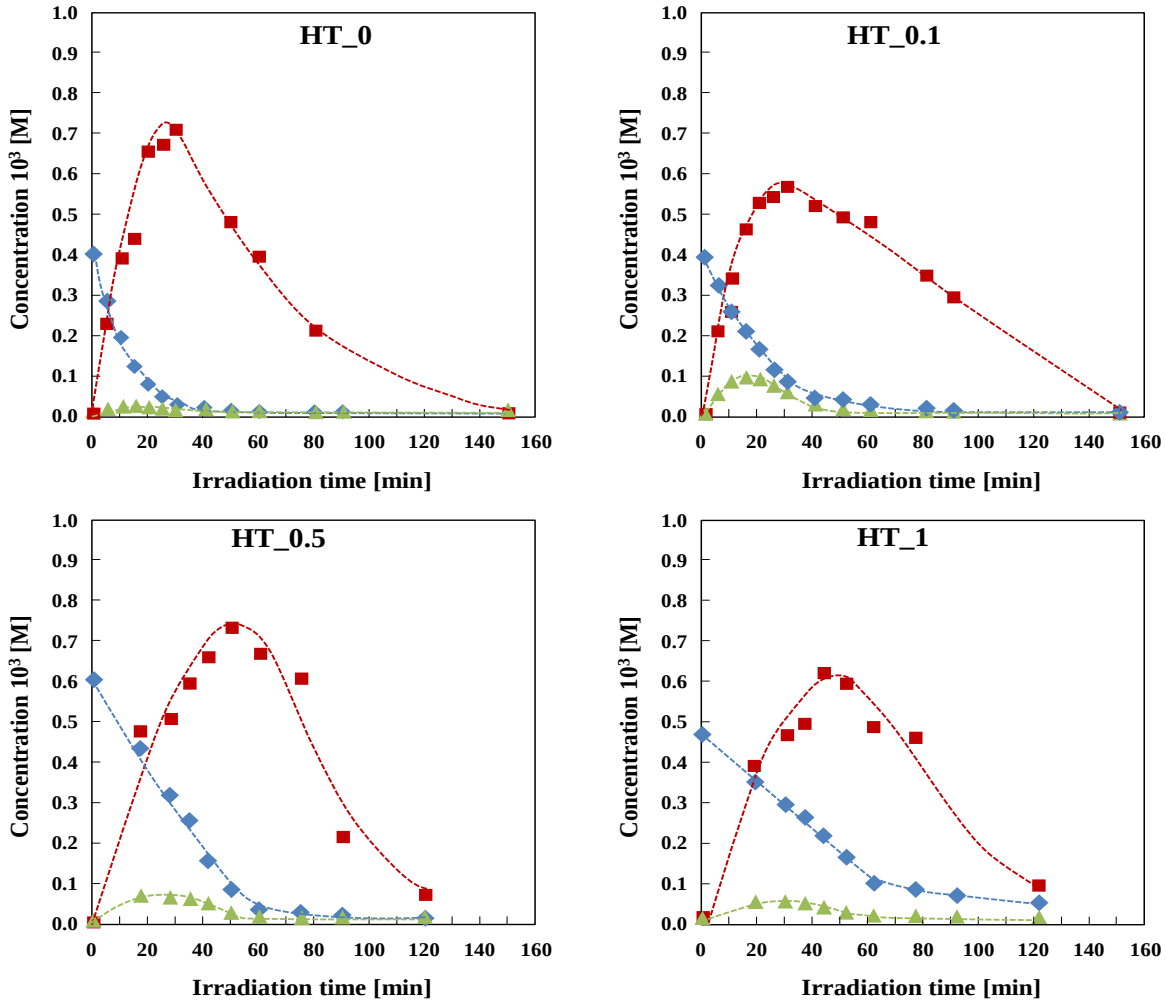

Figure 4. Time-course of (♦) 2-propanol, (■) propanone and (▲) acetaldehyde concentration vs. time under simulated solar radiation in 2-propanol photocatalytic oxidation in the presence of the uncalcined photocatalysts.

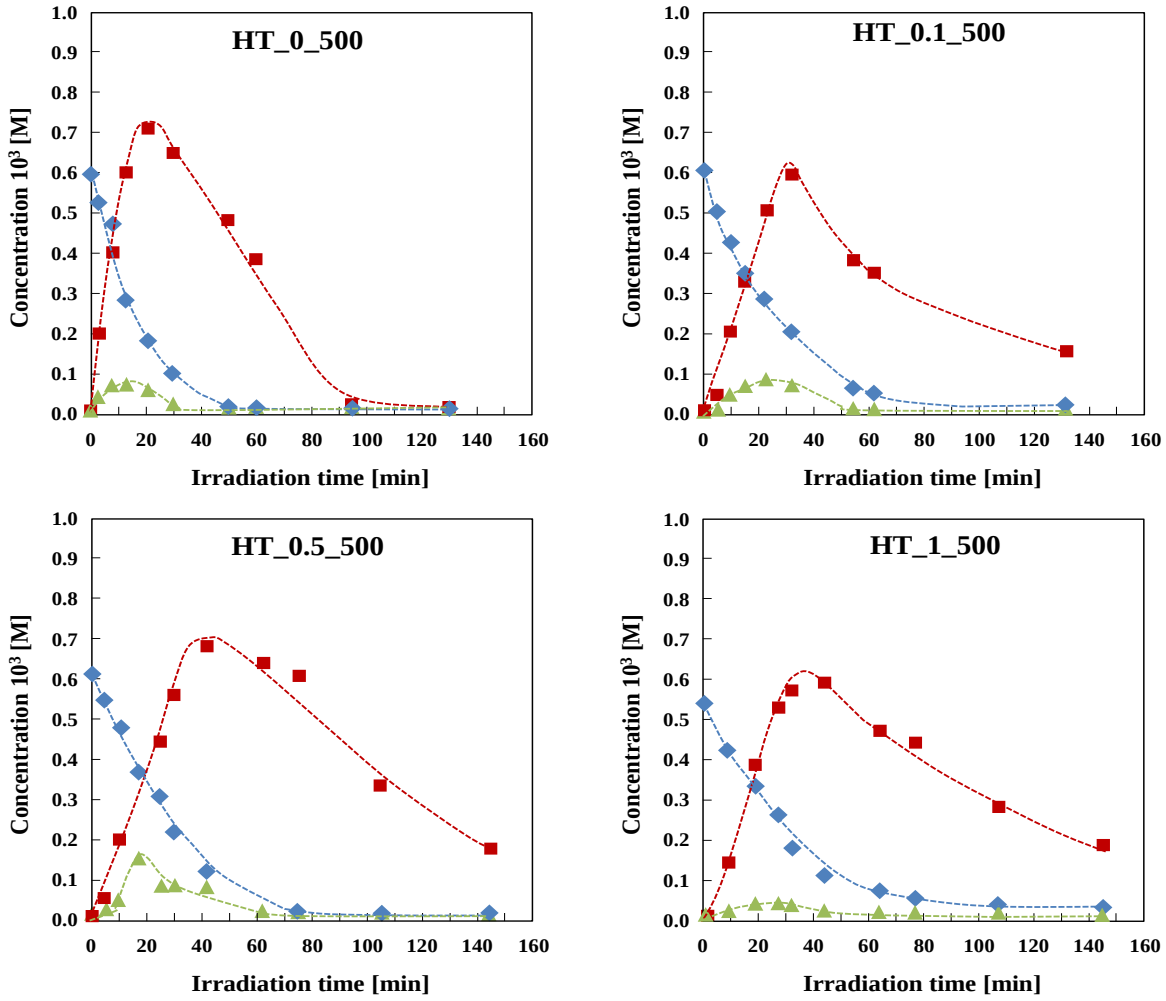

Figure 5. Time-course of (♦) 2-propanol, (■) propanone and (▲) acetaldehyde concentration vs. time under simulated solar radiation in 2-propanol photocatalytic oxidation in the presence of the calcined photocatalysts.

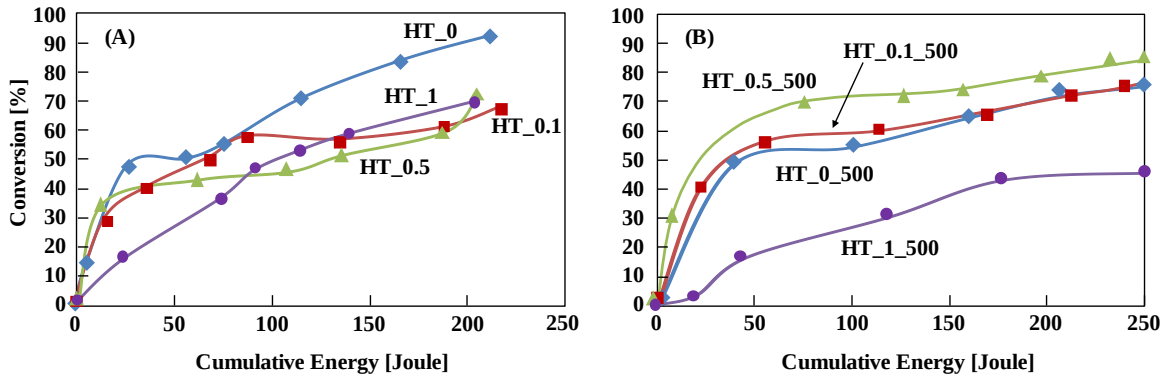

Figure 6. Time-course of propene conversion vs. the cumulative photon energy (naural solar radiation) in the presence of (A) non calcined photocatalysts (♦) HT_0; (■) HT_0.1; (▲) HT_0.5; (●) HT_1, and (B) calcined photocatalysts (♦) HT_0_500; (■) HT_0.1_500; (▲) HT_0.5_500; (●) HT_1_500.